



Review

# What Drives Symbiotic Calcium Signalling in Legumes? Insights and Challenges of Imaging

Teresa Vaz Martins <sup>1,\*</sup> and Valerie N. Livina <sup>2</sup>

<sup>1</sup> Computational and Systems Biology, John Innes Centre, Norwich Research Park, Norwich NR4 7UH, UK

<sup>2</sup> Data Science Group, National Physical Laboratory, Hampton Road, Teddington, Middlesex TW11 0LW, UK; valerie.livina@npl.co.uk

\* Correspondence: tvazmarti@gmail.com

Received: 28 February 2019; Accepted: 30 April 2019; Published: 7 May 2019



**Abstract:** We review the contribution of bioimaging in building a coherent understanding of  $\text{Ca}^{2+}$  signalling during legume-bacteria symbiosis. Currently, two different calcium signals are believed to control key steps of the symbiosis: a  $\text{Ca}^{2+}$  gradient at the tip of the legume root hair is involved in the development of an infection thread, while nuclear  $\text{Ca}^{2+}$  oscillations, the hallmark signal of this symbiosis, control the formation of the root nodule, where bacteria fix nitrogen. Additionally, different  $\text{Ca}^{2+}$  spiking signatures have been associated with specific infection stages. Bioimaging is intrinsically a cross-disciplinary area that requires integration of image recording, processing and analysis. We used experimental examples to critically evaluate previously-established conclusions and draw attention to challenges caused by the varying nature of the signal-to-noise ratio in live imaging. We hypothesise that nuclear  $\text{Ca}^{2+}$  spiking is a wide-range signal involving the entire root hair and that the  $\text{Ca}^{2+}$  signature may be related to cytoplasmic streaming.

**Keywords:** imaging;  $\text{Ca}^{2+}$ ; legumes; *Rhizobium*; symbiosis

## 1. Introduction

Nitrogen is the most common limiting nutrient for plant growth, but a particular class of plants, legumes, can overcome this limitation with the help of bacteria [1,2]. Legumes secrete flavonoids, which are recognised by soil bacteria called rhizobia. In response, rhizobia release Nodulation (Nod) factors. This exchange of signals marks the beginning of a symbiotic relationship. Typically, the root hair tip swells and curls to entrap the bacteria (see Figure 1), which then enter the root upon the formation of a plant-made tunnel-like structure called the infection thread. This allows the bacteria to cross several cell layers. The process culminates in the formation of a nodule, where bacteria will fix nitrogen for the plant in exchange for sugars. Throughout rhizobial infection and the organogenesis of the nodule, the generation and decoding of biochemical signals tells the plant what to do, and central to this process are  $\text{Ca}^{2+}$  signals.

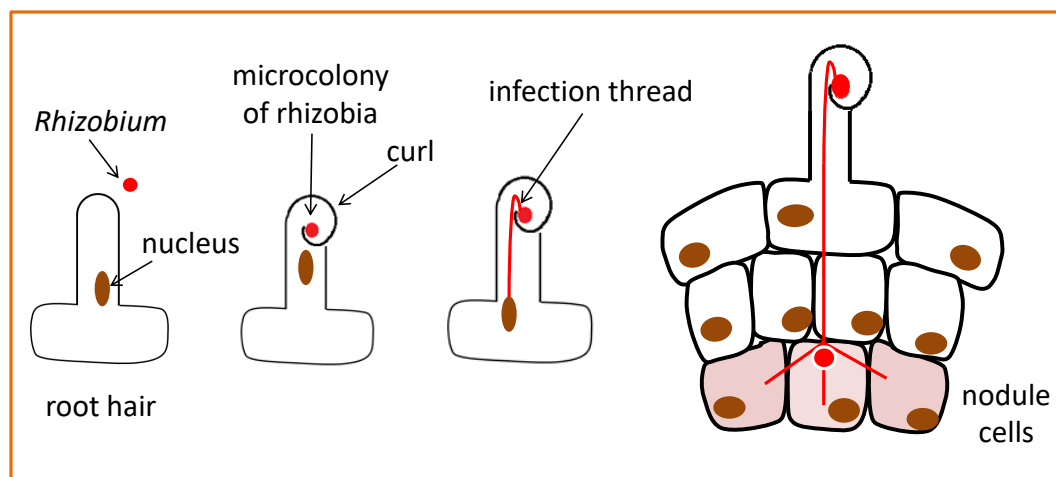


**Figure 1.** Diagram of the response of a *Medicago truncatula* legume root to nitrogen-fixing rhizobia. After exposure to rhizobial signals (Nod factors) the legume root hair curls to entrap the bacteria, which then penetrate into the root via a plant-made infection thread. Branches of the infection thread penetrate cortical cells, which proliferate, leading to the formation of a root nodule to house the bacteria. Nodule formation takes place over the course of several days, while imaging is usually done only for a few hours after root hairs' exposure to Nod factors.  $\text{Ca}^{2+}$  signals have been linked to the infection thread growth and nodule formation by analysis of different mutants. The brown oval denotes the nucleus, which moves to guide the formation of the infection thread [3,4]. The nucleus is anchored by cytoplasmic strands that connect it to the cytoplasm (not represented; it presents different cytoarchitecture according to the root hair development stage).

Investigations into the role of symbiotic calcium signalling integrate knowledge from different disciplines, from genetics to electrophysiology, mathematical modelling and bioimaging. Traditionally, the detection of  $\text{Ca}^{2+}$  signals relied on the use of  $\text{Ca}^{2+}$ -selective microelectrodes, which recorded  $\text{Ca}^{2+}$  currents at one cellular point at a time. With the development of fluorescent calcium sensors, live imaging has revealed diverse spatiotemporal  $\text{Ca}^{2+}$  dynamics [5–9]. This has profoundly impacted the field, as it indicated where to look for the components of the  $\text{Ca}^{2+}$  signalling machinery. This inspired mathematical models [10,11], which attempted to explain the generation of  $\text{Ca}^{2+}$  signals.

The goal of this review is to revisit the contribution to current knowledge about  $\text{Ca}^{2+}$  signals during legume-bacteria symbiosis, from the point of view of bioimaging. Various reviews describe the field from different angles [1,2,12–15]. Bioimaging is special in that it crosses different disciplines and is now being taken to a new level by crucial advances in image processing and quantification [16,17]. It is timely to revisit the imaging evidence obtained so far and identify blind spots that demand a fresh look. Here, we will focus only on the conclusions drawn from fluorescent microscopy.

Rhizobia commonly invade legumes via their root hairs, as shown in Figure 1. In this case, the primary regions of interest are the root hair tip that curls to entrap bacteria and the nucleus where transcription takes place. Bioimaging suggests that there are distinct  $\text{Ca}^{2+}$  signals predominantly associated with each region: a  $\text{Ca}^{2+}$  influx at the tip region, which is thought to be involved in the formation of an infection thread, and nuclear  $\text{Ca}^{2+}$  oscillations, which are required for infection thread growth and nodule organogenesis. Evidence from time-lapse imaging shows the existence of diverse patterns of spatiotemporal  $\text{Ca}^{2+}$  signals, known as  $\text{Ca}^{2+}$  signatures [18–21], such that representative  $\text{Ca}^{2+}$  patterns can possibly be associated with different mutants, infection stages, or outcomes.

It is not trivial to compare  $\text{Ca}^{2+}$  signals in different regions of the cell. Genetically-Encoded  $\text{Ca}^{2+}$  Indicators (GECIs) [22] are increasingly popular largely because, in comparison with dyes, they are easier to target in different cellular compartments. One challenge is that the detected fluorescence depends on the number of fluorophores in the confocal volume of detection, which in turn depends on the cell thickness and cellular motions in and out of focus. Motions include

root hair cytoplasmic streaming, which changes patterns as the root hair grows, causing changes in the distribution of cytoplasmic sensors. To compare  $\text{Ca}^{2+}$  transients in different cellular regions, researchers measure ratios of fluorescence intensity instead of absolute values [23]. This can be done by using ratiometric indicators, such as Fura-2 or calcium cameleons [24,25] or by making pseudo-ratiometric measures when co-loading a non-ratiometric indicator such as calcium green or Oregon green with a  $\text{Ca}^{2+}$ -insensitive reference dextran, such as Texas red.

In any image, the  $\text{Ca}^{2+}$  signal must be detected over the background of fluorescent noise, generated by the detector or arising from the random nature of photon release [26]. The overall ability to detect the signal can be determined by considering the ratio of the signal-to-noise levels of the image [27]. Whether ratiometric or not,  $\text{Ca}^{2+}$  indicators are only effective if there is a sufficient signal-to-noise ratio. Although some characteristics of  $\text{Ca}^{2+}$  signals have been confirmed using several different sensors, imaging processing methods have not been validated by independent approaches, as reliable signal processing methods are still in their infancy in this field. This review will provide examples of how implicit assumptions in image processing and analysis can bias the images we see.

## 2. Two Symbiotic Calcium Signals

In Sections 2.1 and 2.2, we review the  $\text{Ca}^{2+}$  signal responses currently associated with two processes: formation of an infection thread and nodule organogenesis (Figure 1). Table 1 summarises published results regarding two different  $\text{Ca}^{2+}$  signals during this symbiotic interaction. We distinguish two basic different signals.  $\text{Ca}^{2+}$  oscillations are predominantly associated with the nuclear region and a single  $\text{Ca}^{2+}$  fluctuation ( $\text{Ca}^{2+}$  flux) with the tip region. This is a simplified view, as there are areas of intersection: both in terms of response patterns and in terms of location.

**Table 1.** Two different  $\text{Ca}^{2+}$  signals induced by Nod factors were detected in several model legumes, with different  $\text{Ca}^{2+}$  sensors.

LOCATION	RESULT	SPECIES	SENSOR
<b>CALCIUM AT THE TIP</b>			
Cytosol	Apical $\text{Ca}^{2+}$ gradient	<i>Phaseolus vulgaris</i>	Fura-2 [28]
	In growing root hairs, even without Nod factor, in those terminating growth with Nod factor	<i>Vicia sativa</i>	Indo-1 [29]
	Apical $\text{Ca}^{2+}$ plateau-like increase	<i>Vigna unguiculata</i>	Fura-2 and Fluo-3 [30]
	Requires larger Nod factor concentrations	<i>Medicago truncatula</i>	Calcium green/TR [31]
			YC2.1 [32]
		<i>Lotus japonicus</i>	OG-TR [33]
	Flux propagates towards perinuclear region	<i>Medicago truncatula</i>	Calcium green/TR [31]
<b>CALCIUM AT THE PERINUCLEAR REGION</b>			
Nucleus	$\text{Ca}^{2+}$ release at the periphery	<i>Medicago truncatula</i>	Nup YC2.1 [34,35]
		<i>Medicago sativa</i>	Fura-2 [36]
Cytosol/Nucleus	Perinuclear region	<i>Phaseolus vulgaris</i>	Fura-2 [28]
		<i>Pisum sativum</i>	OG/TR [37]
		<i>Lotus japonicus</i>	OG-TR [33]
			Spikes propagate towards tip
Nucleus vs. cytosol	Hotspots	<i>Phaseolus vulgaris</i>	Fura-2 [28]
	Synchronous spikes	<i>Medicago truncatula</i>	70kDaOG, 10kDaRhoD [35]
	Cytosolic $\text{Ca}^{2+}$ spikes delayed		R-GECO, G-GECO [38]
		Cytosolic $\text{Ca}^{2+}$ spikes more symmetric	<i>Lotus japonicus</i>

### 2.1. $\text{Ca}^{2+}$ Spiking Around and Inside the Nucleus

Nuclear  $\text{Ca}^{2+}$  oscillations (or *spiking*) are a distinctive feature of symbiotic  $\text{Ca}^{2+}$  signalling [13,39], observed as a series of high-amplitude signals approximately ten minutes after exposure to

concentrations of Nod factor as low as  $10^{-12}$  M [31,32]. Rather than looking like smooth sinusoidal waves, oscillations occur as repeated asymmetric  $\text{Ca}^{2+}$  peaks, with a rapid rising phase followed by a more gradual decline [36] (see the golden trace in Figure 5A). Because of the universally-asymmetric  $\text{Ca}^{2+}$  spike shape, it is common to refer to  $\text{Ca}^{2+}$  oscillations in *Rhizobium*-legume symbiosis as  $\text{Ca}^{2+}$  spiking. Although adjacent cells do not oscillate in synchrony [25,34], they mostly share similar frequencies and spike shapes. As it is typical in plants, the dynamics of  $\text{Ca}^{2+}$  oscillations are much slower than in the animal field [40]. In the model legume *Medicago truncatula*, the typical  $\text{Ca}^{2+}$  oscillations periods vary between 50 and 100 s.

Perinuclear  $\text{Ca}^{2+}$  spiking is a common response to rhizobial signals in legumes. It was observed at pre-infection stages in legumes that form indeterminate nodules, such as *Medicago truncatula* [41–43], *Medicago sativa* (alfalfa) [36] or *Pisum sativum* (peas) [37], as well as in legumes like *Phaseolus vulgaris* (beans) [28] and *Lotus japonicus* [33,44] that form determinate nodules. It was also observed in *Sesbania rostrata* [45], a legume that can undergo intercellular lateral basal bacterial invasion in addition to the root hair invasion. Perinuclear  $\text{Ca}^{2+}$  spiking persists for some time during trans-cellular infection, as confirmed in *Medicago truncatula* [46].

In all cases, the oscillations appear sharper near the root hair nucleus [36,37], tending to become imperceptible with the distance from it: when  $\text{Ca}^{2+}$  spikes are visible at the tip, the spike rising phase appears more gradual [25]. Possibly [25], this difference reflects  $\text{Ca}^{2+}$  release from sources at the nuclear region and its dissipation as it propagates towards the root hair tip. An alternative hypothesis is that since the cytosol is disproportionately concentrated around the nucleus [37], farther from the nucleus, the fluorescent cytosolic  $\text{Ca}^{2+}$  signal becomes masked by noise. Naturally, the independence of ratiometric techniques from the sensor distribution is only valid assuming that the concentration of the sensors is large enough to allow a good signal-to-noise ratio.

To find the origin of perinuclear spiking, it seemed natural to look around its vicinity, starting from inside the nucleus itself [34]. Whilst several of the dyes previously used did not discriminate between nucleus and cytosol [39], Sieberer et al. [34] used a genetically-encoded yellow cameleon, NupYC2.1, specifically targeted to the nucleus. They reported sustained and regular intranuclear  $\text{Ca}^{2+}$  spiking in the nuclei of *Medicago truncatula* root hairs treated with Nod factors. In terms of frequency and asymmetric spike shape, the characteristics of intranuclear  $\text{Ca}^{2+}$  oscillations were similar to those [36] of perinuclear cytosolic  $\text{Ca}^{2+}$  signals. Spatially, they observed that the intranuclear  $\text{Ca}^{2+}$  concentration was unevenly distributed, and they suggested that each spike originated from the periphery of the nucleus. That could indicate a nuclear envelope  $\text{Ca}^{2+}$  store, and the idea is reinforced by similar imaging results with pseudo-ratiometric indicators [35], as well as by the localisation of the components of a calcium signalling machinery in the nuclear membranes [35,47,48]. Sieberer et al. [34] noted that the uneven distribution of intranuclear  $\text{Ca}^{2+}$  could result from the signal-free nucleolus, but also indicate the presence of possible intranuclear release sites. Regardless of its spatiotemporal signature, the main result in Sieberer et al. [34] was to confirm the existence of intranuclear  $\text{Ca}^{2+}$  spiking.

Since nuclear and cytosolic signals have quite similar time dynamics [35], the nucleus is porous [49] and the nuclear envelope consists of a double membrane with some components of the  $\text{Ca}^{2+}$  signalling machinery on both the cytosolic- and the nuclear-facing side [35,48], cytosolic and nuclear  $\text{Ca}^{2+}$  signals might be coordinated. Whilst a previous study [35] could not discriminate between a cytosolic and nuclear  $\text{Ca}^{2+}$  origin, recently [38], an important step was made with the development of new genetically-encoded calcium sensors, GECOs, with a much improved dynamic range. Using a dual colour sensor able to detect cytosolic and intranuclear  $\text{Ca}^{2+}$  signals simultaneously, Kelner et al. [38] reported that the majority of perinuclear cytosolic  $\text{Ca}^{2+}$  spikes started with a delay relative to nuclear  $\text{Ca}^{2+}$  spikes. However, it was not possible to distinguish between nuclear and cytosolic  $\text{Ca}^{2+}$  spiking initiation sites clearly in 30% of cases, and in very few cases (2%), intranuclear  $\text{Ca}^{2+}$  spikes appeared delayed relative to perinuclear  $\text{Ca}^{2+}$  spikes. In time-lapse live imaging, it can be very challenging to delineate boundaries of small regions. In the study [38], the authors chose an oval as the region of interest to represent the nucleus, while the perinuclear region was represented by an

annular-shaped region of interest around the nucleus. Both regions of interest appeared static, which can potentially lead to partial loss of the signal if the nucleus or the root hair moves slightly, especially for the case of the narrow annular-shaped perinuclear region of interest. Perhaps the percentage of inconclusive results could be settled by the choice of larger/dynamic regions of interest for the perinuclear region. In case the thickness and position of the confocal slice allows the observation of overlapping nuclear and cytosolic signals, the nuclear and perinuclear regions of interest can even coincide, taking advantage of the ability of the sensor to discriminate between nuclear and cytosolic signals.

## 2.2. $Ca^{2+}$ Levels Rise at the Root Hair Tip

When legume root hairs are exposed to low ( $10^{-12}$  M) concentrations of Nod factor, spiking is the only  $Ca^{2+}$  signalling response, which occurs within 10 minutes of Nod factor application. By contrast, high ( $>10^{-9}$  M) concentrations of Nod factor induce an immediate  $Ca^{2+}$  flux, which is described as a rapid rise in cytoplasmic  $Ca^{2+}$  concentration at the root hair tips followed by slower decline to baseline calcium levels [28–33,37,50].  $Ca^{2+}$  flux can last up to 10 minutes and is followed by  $Ca^{2+}$  spiking [31,32] as well.

While imaging evidence shows an immediate  $Ca^{2+}$  flux followed by  $Ca^{2+}$  spiking, it is thought that the  $Ca^{2+}$  flux occurs later than  $Ca^{2+}$  spiking in natural conditions [33]. There is no contradiction here, as  $Ca^{2+}$  flux can be induced in root hair cells that are already spiking if the concentration of Nod factor is raised later in the experiment [31,37]. When does the concentration of bacterial signals increase in natural settings? Miwa et al. [33] noted that the concentration of Nod factors will likely be low during the first contact between *Rhizobium* and the legume root hair. Combining imaging and genetic evidence, they proposed that  $Ca^{2+}$  spiking would be the only  $Ca^{2+}$  signalling response at this early stage, along with root hair deformation that precedes curling; see Figure 1. Then, the Nod factor concentration is raised by the increasing number of rhizobia growing within the enclosed root hair curl, and that triggers a  $Ca^{2+}$  flux.

Combining evidence from imaging with the design of mutants with different impairments, it is suggested that apical  $Ca^{2+}$  flux is related to the activation of infection thread growth [33]. Imaging studies support this picture on several grounds. While an apical  $Ca^{2+}$  gradient is observed in developing root hairs even in the absence of Nod factor, the root hairs that are terminating growth respond to Nod factor not only by a  $Ca^{2+}$  flux, but also by recovering additional characteristics associated with tip-growing cells, namely a polar cytoplasmic organisation and reverse fountain streaming [29]. Notably, it is at this stage of development that the root hair is more susceptible to rhizobial infection [51]. Indeed, apical  $Ca^{2+}$  signals are associated with growth in several plants [52,53]. For its part, nuclear  $Ca^{2+}$  oscillations are a distinctive feature of symbiotic  $Ca^{2+}$  signalling required for infection thread growth and also for nodule morphogenesis [36,37,41], which along with infection thread growth is a developmental program required for the nitrogen-fixing nodules.

Besides having different temporal dynamics,  $Ca^{2+}$  flux and  $Ca^{2+}$  spiking responses are associated with different spatial cellular regions:  $Ca^{2+}$  flux with root hair tip, and  $Ca^{2+}$  spiking with the nuclear region. Currently, it is thought that the  $Ca^{2+}$  signals propagate passively along the root hair. Thus, it was reported that each perinuclear  $Ca^{2+}$  spike is reproduced along the root hair, with a delay that increases with the distance from the nucleus [31,38]. By contrast, the  $Ca^{2+}$  flux originates at the tip and appears delayed as it propagates towards the nucleus [31].

## 3. Calcium Signatures

Bioimaging has shown that  $Ca^{2+}$  signals can adopt rich spatiotemporal patterns, each known as a different  $Ca^{2+}$  signature. In some plants and animals, calcium spatio-temporal patterns can encode information about the primary stimuli, and the attribution of coding properties to calcium signals inspired the search for representative calcium traces. Among other characteristics, the so-called *calcium signatures* can have different frequencies or spike shapes and can be typical of different root hair

development stages [42], infection stages [46], or different bacterial invasion strategies [45]. Table 2 lists some of the biological phenomena in rhizobial-legume symbiosis that have been associated with different  $\text{Ca}^{2+}$  signatures.

**Table 2.** Calcium signatures: different  $\text{Ca}^{2+}$  oscillation frequencies or spike shapes characterise different phenomena.

CALCIUM SIGNATURES			
COMPARISON	RESULT	SPECIES	SENSOR
Infection thread growth rate	Frequency increases in periods of rapid elongation		NupYC2.1 [54]
Transinfection stage	Frequency increases when transcellular infection starts	<i>Medicago truncatula</i>	YC2.1 <sub>cyt</sub> YC3.60 <sub>cyt</sub> NupYC2.1 [46]
Myc and NF	Deterministic chaotic patterns		YC2.1 [55]
Root hair development stage	Slower frequency in younger root hairs		YC2.1 [42]
$\text{Ca}^{2+}$ sensors $k_d$	Spike shape: decay phase more gradual for smaller $k_d$		OG/TR vs. YC2.1 [56]
Invasion mode	Frequency faster in the lateral root base than root hair invasion mode	<i>Sesbania rostrata</i> <i>Medicago truncatula</i>	OG and TR [45]

### 3.1. $\text{Ca}^{2+}$ Frequency

In legume-microbe symbiosis, calcium signals are part of a biochemical signalling pathway, with several components shared with another symbiosis that most plants establish with Mycorrhizal (Myc) fungi to meet their demands for phosphorus. An attractive hypothesis is that  $\text{Ca}^{2+}$  signals encode specific information about the primary stimuli, either fungal Myc factors or bacterial Nod factors. However, although one study [55] suggested that Myc and Nod factors induce different  $\text{Ca}^{2+}$  signatures with a flexibility provided by their deterministic chaotic nature, the authors noted that different experimental approaches may have played a part in the results. While doubts remain about the specificity of  $\text{Ca}^{2+}$  signatures during pre-infection, at later symbiosis stages, the patterns of  $\text{Ca}^{2+}$  oscillations are similar in both Myc and Nod symbioses and related instead to the stage of infection [46]: in both symbioses,  $\text{Ca}^{2+}$  spiking switches from infrequent and irregular, to a pattern of high-frequency regular oscillations when transcellular infection begins [46].

In a study by Sieberer et al. [46], the period of rapid spiking associated with apoplastic cell entry lasted for a total of 35–45 consecutive spikes, a similar number to the about 36 consecutive  $\text{Ca}^{2+}$  spikes predicted to be critical for regulating the ENOD11 gene activation involved in nodulation [42]. In fact, simple mathematical models [57] propose explanations for decoding mechanisms based, among other features, on the number of spikes. Whereas  $\text{Ca}^{2+}$  spiking stops before transcellular infection has finished [46], it lasts for the entire duration of bacterial progression through the infection thread at the root hair [54], with faster frequencies when the rate of elongation is more rapid. If the growth of the infection thread stops, nuclear  $\text{Ca}^{2+}$  spiking is not observed [54].

Besides being related to infection stages in bacteria-legume symbiosis [46,54], the frequency of  $\text{Ca}^{2+}$  oscillations increases with the age of the root hair [42] and is also related to the bacterial mode of invasion. Bacterial infection via root hair invasion is common in legumes, but a few legumes can also nodulate at lateral root bases via a form of crack entry. Such is the case for the semi-aquatic legume *Sesbania rostrata*, capable of experiencing either mode of invasion. While oscillations associated with root hair invasion on growing root hair cells are comparable in *Sesbania rostrata* and *Medicago truncatula* [45], the frequency of perinuclear calcium oscillations is faster and each spike more symmetric when *Sesbania rostrata* is nodulated at lateral root bases.

Note that despite the notion of characteristic oscillation frequencies, an oscillation frequency may vary with time. For instance, the onset of a more or less regular period of  $\text{Ca}^{2+}$  oscillations is often

preceded by a period of initial rapid spiking, which can be stimulated again by repeated addition of Nod factor [56].

### 3.2. The Shape of Calcium Spikes

A typical symbiotic calcium spike induced by Nod factor is asymmetric [36], with a rapid rising phase (1–4 s) followed by a more gradual decline that lasts more than 30 s. This is thought to correspond to the opening of calcium release channels, followed by the slower pumping of calcium back into  $\text{Ca}^{2+}$  stores.

As expected, the speed of the decay phase depends on the equilibrium dissociation constant ( $K_d$ ) of the  $\text{Ca}^{2+}$  indicator [42,56]. An indicator senses calcium by binding free calcium. In the wider context of buffering effects, calcium binding leads to the removal of free calcium, just as a pump would. The ratiometric cameleon sensor YC2.1 (YFP/CFP) reports a faster  $\text{Ca}^{2+}$  spike decline and has a larger  $K_d$  for  $\text{Ca}^{2+}$ , than the dye Oregon Green used with the reference Texas Red (OG/TR). Using realistic  $K_d$  appropriate for each sensor, Granqvist et al. [56] were able to fit spikes detected with the different sensors. Besides the different  $K_d$ , Texas red is a reference dye insensitive to calcium, while CFP intensity decreases with calcium binding (Figure 2). More detailed spike shape analysis could consider the effects of comparing a ratiometric with a pseudo-ratiometric technique, in particular in very noisy images.

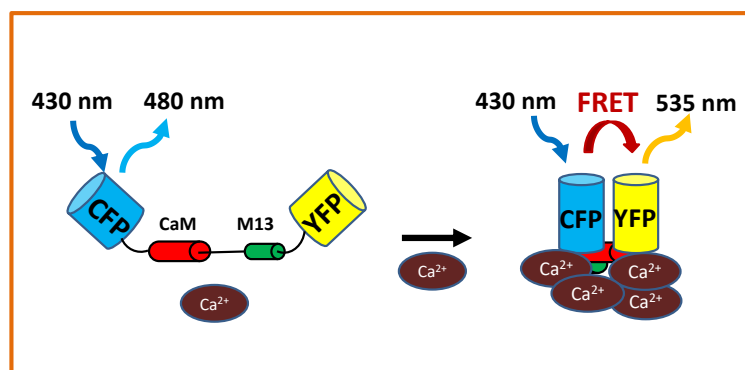


**Figure 2.** Yellow cameleons are  $\text{Ca}^{2+}$  sensors based on Förster Resonance Energy Transfer (FRET). Yellow and Cyan Fluorescent Proteins (YFP and CFP) are mutated forms of the green fluorescent protein that absorb and emit light at matching wavelengths, such that the excitation wavelength of YFP is the emission wavelength of CFP. The sensor is constructed by attaching CFP and YFP by the  $\text{Ca}^{2+}$ -binding protein Calmodulin (CaM) and a calmodulin binding peptide (M13) [24]. When  $\text{Ca}^{2+}$  concentration increases, CaM undergoes a conformational change as it binds to  $\text{Ca}^{2+}$ , which brings YFP and CFP closer together and results in enhanced FRET. At the level of a single yellow cameleon construct, a rise in  $\text{Ca}^{2+}$  concentration is indicated by a drop in the CFP intensity at the same time that the YFP intensity increases, leading to an increase of the YFP/CFP ratio.

Using similar calcium sensors, spike shape analysis can be applied to detect  $\text{Ca}^{2+}$  spikes [34] or as yet another characteristic to evaluate  $\text{Ca}^{2+}$  signatures [25,43,45].

## 4. Imaging $\text{Ca}^{2+}$ Spiking

The scenario that emerged from imaging studies is of two independent symbiotic calcium signals each predominantly associated with different locations: a  $\text{Ca}^{2+}$  flux that begins at the root hair tip and nuclear  $\text{Ca}^{2+}$  oscillations that initiate from the nucleus periphery. To compare signal intensity in cellular regions with different proportions of calcium sensors, researchers use ratiometric sensors.

In live imaging, the fluorescence signals are often very weak, but options to amplify the signal and obtain an image with a good signal-to-noise ratio may conflict with requirements to keep the specimen healthy and optimise the spatiotemporal resolution. Several studies [25,34,35,38] adopted confocal

microscopy [58], a technique that enhances optical resolution by the use of a spatial pinhole to remove out-of-focus light. In case the fluorescent signal is very weak, it is possible to capture more signal by increasing the size of the pinhole, but the added signal will arrive from out-of-focus planes, blurring the image. In Confocal Laser Scanning Microscopy (CLSM), the image is built by a point-by-point scan, and the first and last scanned pixel in an image frame may be separated by seconds or milliseconds. To amplify the signal, we can scan a line several times and then average the image into one, but that is done at the expense of the temporal resolution, which in turn can be increased if we decrease the pixel dwell time, but this again will decrease the signal. If the laser power is increased to amplify the signal, there is a risk of photobleaching and cell damage. To summarise, live imaging is technically difficult, and each particular experiment requires different trade-offs. It may not compensate to increase the signal intensity beyond a certain point, and in that case, imaging processing tools need to tackle the effects of a low signal-to-noise ratio.

In what follows, we will show how imaging processing options impact the visual appearance and interpretation of the imaging evidence. We will use examples of calcium signals induced by  $10^{-9}$  M Nod factor in *Medicago truncatula* root hairs. We imaged the root hairs using a confocal microscope (Zeiss Axio Imager Z2 upright microscope, LSM 780), and as  $\text{Ca}^{2+}$  sensors, we used members of the Yellowameleon (YC) family of genetically-encoded calcium sensors, specifically YC2.1 (Figures 4 and 5) and YC3.6 (Figures 6 and 8). The YC2.1 and YC3.6 cameleons are constructed with a fixed 1:1 stoichiometry of a single donor and acceptor, CFP and YFP, attached to a calcium-binding molecule (see Figure 2). As their relative abundance is the same, the ratio between YFP and CFP should in theory be independent of the expression level, with an increase in the ratio of emission at the two wavelengths (YFP/CFP) indicating a relative increase of the  $\text{Ca}^{2+}$  concentration.

However, digital images are made up of pixels, and the intensity of a pixel is composed of the signal from the sensor plus a random number corresponding to detector or sample noise. A general rule is that the proportion of signal-to-noise ratio is smaller for weaker signals [26]. The challenge is that the cellular regions to compare (nucleus vs. tip, or nuclear periphery vs. interior) may have very different signal-to-noise ratios. If this is not dealt with, results may be misleading.

Photobleaching is a common feature in fluorescence microscopy, weakening the signal over time as the fluorophores start losing the ability to fluoresce. However, in live imaging, the ever-changing signal-to-noise ratio appears more complex than a monotonous decay and can pose a hidden complication. Figure 3 shows an idealised representation of any generic cellular object and its corresponding microscopic digital image. The signal (and thus, the signal-to-noise ratio) depends on continuous cellular motions and shape changes. If our region of interest is static while the cellular object moves, the signal and thus the signal-to-noise ratio fluctuate alongside variations of the sensor-labelled cytoplasm/nucleus in view. Disregarding shape effects, the problem could be solved by creating a binary signal/noise image and restricting measures to the dynamic region of interest classified as the signal. However, we need to take into account the shape of the object, and in particular its edges and interfaces. Any cellular object (e.g., nucleus or cytoplasmic strands) is delimited by relatively smooth edges, and the corresponding signal intensity in its 2D representation will be weaker near edges: see the 2D signal corresponding to the sharpest edge at the left (Figure 3A). Furthermore, often, movements and shape changes go together, and all this can be made even more complicated by an uneven local noise from autofluorescent elements. In the simplest case, edges and dynamic cellular regions have a lower signal-to-noise ratio.

With this in mind, we will revisit two phenomena: (1)  $\text{Ca}^{2+}$  release from the nuclear periphery (Section 4.1) and (2) the relation between intranuclear and cytosolic  $\text{Ca}^{2+}$  spiking (Section 4.2). Then, we will see what imaging can tell us about the relation between perinuclear  $\text{Ca}^{2+}$  spiking frequency and other signals at the tip (Section 4.3). The images we used are not meant to be representative of all symbiotic  $\text{Ca}^{2+}$  spiking. Instead, they serve to highlight potential pitfalls in the interpretation of images and to suggest questions for further investigation.

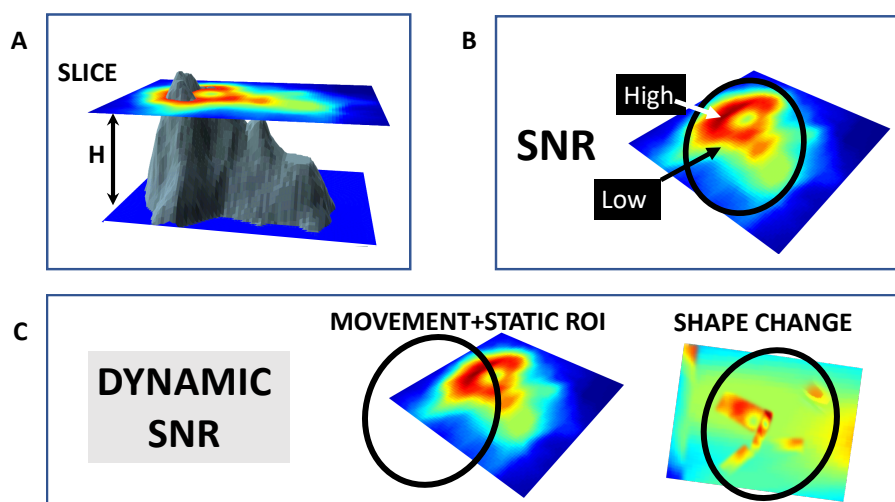


**Figure 3.** The dynamic nature of the signal-to-noise ratio in live imaging. (A) In confocal microscopy, the focal plane is defined by the top of the position of the confocal slice through the object (grey). This slice has a small thickness  $H$ , which determines how much out-of-focus light is detected. (B) The signal-to-noise ratio is higher where the signal is stronger: if the sensor is evenly distributed, the signal-to-noise ratio at a given point reflects the depth/shape of the object at that point. (C) In living samples, the signal-to-noise ratio is constantly changing: it decreases if the signal is lowered because the object moves out of a statically-defined region of interest (oval) or if the shape of the object changes in certain ways, e.g., becoming less compact and thus increasing weak edge effects. The idealised cellular object was created from the R volcano dataset [59], using the plot3D R package [60].

#### 4.1. Do We See Intranuclear Calcium Being Released from the Nuclear Periphery?

From other lines of evidence besides imaging, it appears that  $\text{Ca}^{2+}$  is released at the nuclear periphery [35,47,48]. Nevertheless, imaging remains important to understand the scales of the  $\text{Ca}^{2+}$  spatiotemporal signatures and to pin down the mechanisms of interaction between all the elements involved in  $\text{Ca}^{2+}$  signalling.

Sieberer et al. [34] suggested that the rapid increase in  $\text{Ca}^{2+}$  concentration observed at the start of a  $\text{Ca}^{2+}$  spike happens near the nuclear envelope, while the results of Capoen et al. [35] showed that the nuclear periphery remains brighter throughout the entire spike, as if  $\text{Ca}^{2+}$  never totally engulfed the entire nucleus. Curiously, the signal at the nuclear periphery tends to be more intense even during periods of rest. In Sieberer et al. [34], even in between spikes, we can observe apparent calcium hotspots along the nuclear border or, more rarely, inside the nucleus. Moreover, in Capoen et al. [35], even when the nucleus is not exposed to Nod factor, the border region appears brighter than the interior, although not as bright than when signal-to-noise ratio is present and  $\text{Ca}^{2+}$  is spiking. Why, in both studies [34,35], does the nuclear periphery appear brighter even when a  $\text{Ca}^{2+}$  spike is not imminent? A hypothesis could be that calcium levels were building up at the nuclear border until a threshold was reached when calcium burst into the nucleus, as long as enough resting time had passed and the right stimulus (Nod factor) was present. However, we cannot confirm or discard this hypothesis before addressing the fundamental problem of how to compare different parts of one image that have different signal-to-noise ratios reliably. Imaging  $\text{Ca}^{2+}$  diffusion is not merely a matter of spatiotemporal resolution: as a pre-condition, the  $\text{Ca}^{2+}$  signal needs to be strong enough in different nuclear regions.

We have looked closer at this point using the following example. Figures 4 and 5 refer to the same *Medicago truncatula* root hair exposed to Nod factor, imaged with a confocal microscope. The calcium indicator is the nuclear-targeted yellow cameleon YC2.1. The image  $I_1$  of Figure 4 shows the YFP and CFP intensity distributions at the peak of a  $\text{Ca}^{2+}$  spike. Both YFP and CFP signals are weaker at the nucleolus region and also near the nuclear border. The signal is better captured by a microscope at

the centre of the focal plane, weakening its intensity at the nuclear edges if the nucleus is at the centre of the image. However, even if the nucleus is not at the centre of the image, on a 2D confocal slice, the nucleus periphery will show a weaker signal simply because of edge effects (Section 4, Figure 3). At this point, we have a choice before calculating the ratio YFP/CFP.

**Option A**, upper panel of Figure 4, illustrates the ratio image  $I_{2A}$  obtained without any previous imaging processing. It appears that the  $\text{Ca}^{2+}$  concentration is largest at very small scattered hotspots, some closer to the nuclear edges and some inside (near the nucleolus). However, this picture of  $\text{Ca}^{2+}$  distribution is not reliable because noise from fluorescent images is a much larger component of small values [26,27], and the ratios can become artificially large simply because of the small number of photons involved with high uncertainty. Among the different types of noise in fluorescence microscopy [26,27], shot noise, which originates from the particle nature of light, is the fundamental limit of the signal-to-noise ratio [27]. Shot noise follows a Poisson distribution, for which the standard deviation is equal to the square root of the expected value: although its absolute value decreases with the signal intensity, the signal-to-noise ratio decreases even faster. If we measure a value within one standard deviation of the true  $\text{Ca}^{2+}$  signal, the ratio between equally-large true signals of, for instance, 400 photons will be measured within the range [0.9–1.1], while between true weak signals of four photons will be measured within [0.3–3], from one third smaller to up to almost three-times larger. Visually, this could appear as fluctuating hotspots at the nuclear periphery/nucleolus, even in between calcium spikes and even if we assume for simplicity that the YFP and CFP intensities are the same in those periods of rest (one of the FPs is usually less bright). Therefore, some adjustment should be applied before doing ratios.

**Option B**, lower panel of Figure 4, attempts to follow the recipe provided by Sieberer et al. [34], as closely as we can. The first step is to apply a median filter (Step B<sub>1</sub> in Figure 4). The median filter removes isolated pixels, either outlier noise or small signal details. Compared with Gaussian blurs or mean filters, it is effective at preserving edges when the original image shows a sharp decline in intensity at the border of the object. We can observe its effects if we compare (Figure 4) the YFP and CFP signals, before ( $I_1$ ) and after ( $I_{2B}$ ) filtering. Around the edges, the probability of the signals being outliers is greater, and filtering will not raise intensities at every pixel all around the nuclear periphery. This becomes a problematic region where artefacts arising from the ratio between small random numbers can occur. The nuclear boundary risks being implicitly determined by the statistics of the background noise, which may even vary at different sides of the nucleus (compare YFP, CFP and YFP/CFP nuclear shape; see Figure 5). For the final step before computing the ratio (step B<sub>2</sub> in Figure 4), we followed the formula provided by the RatioPlus ImageJ plugin [61,62]. This plugin calculates the pixel-by-pixel ratio after background subtraction and clipping (if after background subtraction, the pixel intensity is lower than the clipping value for that image, it is set to zero before ratio calculation) [61]. The image frame is assumed to have a homogeneous background, whose value we chose using the intensities at regions away from the nucleus. We also assumed that the background does not change with time, as the plugin can be used on a stack of images simultaneously. To select the clipping value, we took the difference between the measured minimal intensity and the background intensity and divided it by two. Unsurprisingly in our example, after the filtering and RatioPlus steps, the final ratio image ( $I_{3B}$ , Figure 4) showed a much clearer brighter border, compared to the ratio image  $I_{2A}$ .

Such edge artefacts will further be exaggerated if CFP is less intense than YFP and at the time of a  $\text{Ca}^{2+}$  spike. The periphery of the nucleus reported by the CFP signal will appear disproportionately shrunk by the filter + background subtraction procedure (see the colour-bar scale in Figure 5). Then, during a  $\text{Ca}^{2+}$  spike, the CFP signal intensity drops, further worsening its signal-to-noise ratio. That can artificially enhance the ratio YFP/CFP near the periphery of the nucleus during a  $\text{Ca}^{2+}$  spike (Figure 5).

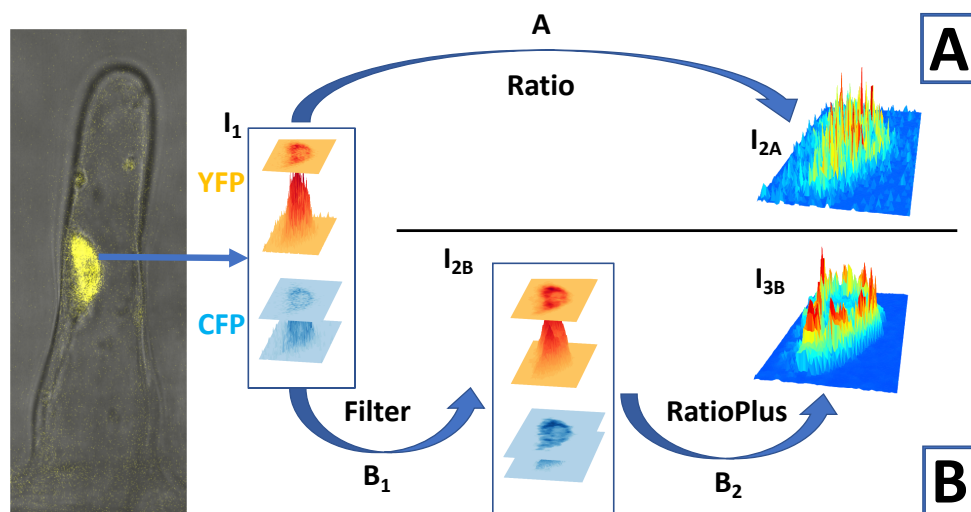


**Figure 4.** Choices in image processing alter the final ratio image, especially at its edge. The position of a nucleus (yellow) in a *M. truncatula* root hair is shown in the bright field image of the root hair (grey), merged with the YFP image. Path **A** shows what happens when images are not processed, while Path **B** attempts to follow the image processing steps reported in Sieberer et al. [34]. The 2D microscope image of the YFP and CFP intensities at the nucleus reflects the 3D structure of the nucleus,  $I_1$  and  $I_{2B}$ . The ratios YFP/CFP of images are  $I_{2A}$  and  $I_{3B}$ . We used the nuclear localised  $\text{Ca}^{2+}$  sensor YC2.1.

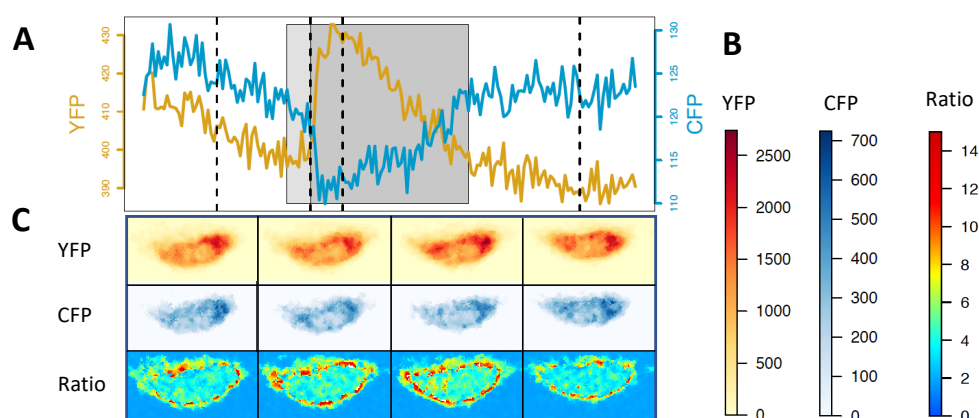


**Figure 5.** Signal enhancement at the nuclear periphery before, during and after a single  $\text{Ca}^{2+}$  spike, when adopting image processing Option B of Figure 4. **(A)** During a  $\text{Ca}^{2+}$  spike (grey rectangle), the CFP intensity (blue) decreases while YFP intensity (red) increases. **(B)** Colour-bars show that the CFP is less bright than the yellow YFP. **(C)** The signal from YFP and CFP is not uniformly distributed across the nucleus and it is weaker at the periphery. These intensities are presented after filtering, background subtraction and clipping (Path B in Figure 4). The ratio YFP/CFP is always brighter at the periphery of the nucleus and even more so during the  $\text{Ca}^{2+}$  spike (two central ratio pictures; Panel (C)). The  $\text{Ca}^{2+}$  spike data were recorded every 0.37 s, and each of the four sequential images for YFP, CFP and ratio in (C) correspond to the vertical dotted lines before, at the onset, at its peak, and after the  $\text{Ca}^{2+}$  spike in (A). The  $\text{Ca}^{2+}$  sensor was the nuclear-localised YC2.1.

The chosen [34] ImageJ RatioPlus plugin assumes a very accurate definition of the region of interest [63,64], such that neither CFP nor YFP signals fall below the intensity threshold that defines background noise. Starting from the same image, in Figure 4, we see two different spatial distributions of  $\text{Ca}^{2+}$  signals,  $I_{2A}$  and  $I_{3B}$ . Neither result is the true one, as neither of them solves the problem of compensating for different spatial distributions of the signal-to-noise ratio, but image  $I_{3B}$  also shows additional edge enhancements.

We do not know how important the edge effects discussed above were for the images presented in the literature [34,35]. However, unless they are addressed with appropriate statistical tools, the  $\text{Ca}^{2+}$  levels measured near the periphery of the nucleus will always be biased, to a degree that will depend on the depth of field in the confocal microscope, the fluorescence levels of the specimen, the background values, etc. To bypass the problem of comparing regions with such different signal-to-noise ratios, we could measure signals well inside the nucleus (barring the nucleolus region) and infer the direction of calcium propagation from diffusion profiles. That would possibly imply imaging at even finer levels of spatiotemporal resolution than used so far [34,35], as a clear diffusion profile becomes unclear once calcium is inside the nucleus.

#### 4.2. Can We See How Apical and Perinuclear $\text{Ca}^{2+}$ Oscillations are Related?

Symbiotic  $\text{Ca}^{2+}$  spiking is currently firmly associated with the nuclear and perinuclear region. In imaging studies, spikes appear delayed with distance from the nucleus [31,38]. Often, the shape of cytosolic calcium spikes degrades and dissipates farther from the nucleus. This makes cytosolic  $\text{Ca}^{2+}$  spiking appear almost like a casual by-product, which if it encoded a message, it would be discarded as meaningless. However, how does a worse signal-to-noise ratio at the root hair tip alter the appearance of  $\text{Ca}^{2+}$  spikes at the tip?

Unless the root hair is so young that it still exhibits a cytoplasmic plug at the tip, the signature of  $\text{Ca}^{2+}$  spiking far from the nucleus is complicated by the impact of cytoplasmic streaming, which constantly rearranges the distribution of  $\text{Ca}^{2+}$  sensors seen in a static region of interest. A clearer signal is expected where  $\text{Ca}^{2+}$  sensors continuously occupy a relatively large and stable region like the nucleus and the cytosol surrounding it. Can the apparent degradation of  $\text{Ca}^{2+}$  signals near the root hair tip be an artefact of cytoplasmic streaming? While  $\text{Ca}^{2+}$  release is indicated by an increase in the ratio YFP/CFP, intracellular motions can possibly cause changes in the signal-to-noise ratio that affect that ratio. When motions within the cell are significant and happen at similar time scales as  $\text{Ca}^{2+}$  release, it may be challenging to disentangle the causes of small YFP/CFP changes. We illustrate this challenge with an example of a *Medicago truncatula* root hair exposed to Nod factor, now using the cytosolic/nuclear  $\text{Ca}^{2+}$  sensor YC3.6 (Figure 6).

We present the  $\text{Ca}^{2+}$  (YFP/CFP) traces, in Panel A  $a_1$ , Figure 6, without any conventional pre-processing: no denoising and no background and trend removal [5,8,65]. As is typical, the  $\text{Ca}^{2+}$  spikes are much sharper at the perinuclear region. However, there are a few atypical observations. The larger peaks of the apical  $\text{Ca}^{2+}$  spikes are not always delayed relative to the corresponding perinuclear  $\text{Ca}^{2+}$  spikes. Furthermore, each  $\text{Ca}^{2+}$  spike at the tip seems composed of a previous spike that happens before the major perinuclear  $\text{Ca}^{2+}$  peak (vertical dotted lines; Panel A  $a_1$ , Figure 6). In fact, the *precursor spike* coincides with a gradual growth of perinuclear  $\text{Ca}^{2+}$  concentration, before the characteristic steep spike rising phase that is reported in the literature.

Note that  $\text{Ca}^{2+}$  signals were imaged in this root hair more than half an hour after exposure to NF, so even if there had been a previous apical  $\text{Ca}^{2+}$  flux (not observed), at this point, we would not expect to observe any interference with the typical  $\text{Ca}^{2+}$  spiking associated with the nucleus. On this account, is the coincidence between the gradual start of the perinuclear  $\text{Ca}^{2+}$  spikes and the existence of *precursor* apical  $\text{Ca}^{2+}$  spikes an artefact? In other words, do the apical YFP/CFP ratio changes indicate real  $\text{Ca}^{2+}$  transients?

If some features of the apical spikes are artefacts caused by the changing distribution of the  $\text{Ca}^{2+}$  sensors, then imaging processing steps that alter the spatial distribution of the YFP and CFP signals could potentially alter the appearance of the time series. Panel B, Figure 6, illustrates the effect of filtering and background subtraction (option *b*), as compared to simple pixel-by-pixel ratio (YFP/CFP) calculation (option *a*). The first observation is that without filtering, the ratio image appears so noisy that we can hardly recognise the cytosol/vacuole interface. Secondly, we see that filtering and background subtraction changes the apical YFP/CFP traces to reveal *bumps* with size and time scales comparable to the apparent apical  $\text{Ca}^{2+}$  spikes. Given this, it would be unclear how to adapt

the usual pre-processing steps, such as trend removal, to these time series. In fact, with this option *b*, the existence of any apical  $\text{Ca}^{2+}$  spikes looks uncertain. However, it is still possible to distinguish apparent apical double  $\text{Ca}^{2+}$  spikes in both (*a* and *b*) cases, which coincide with the perinuclear  $\text{Ca}^{2+}$  spikes.

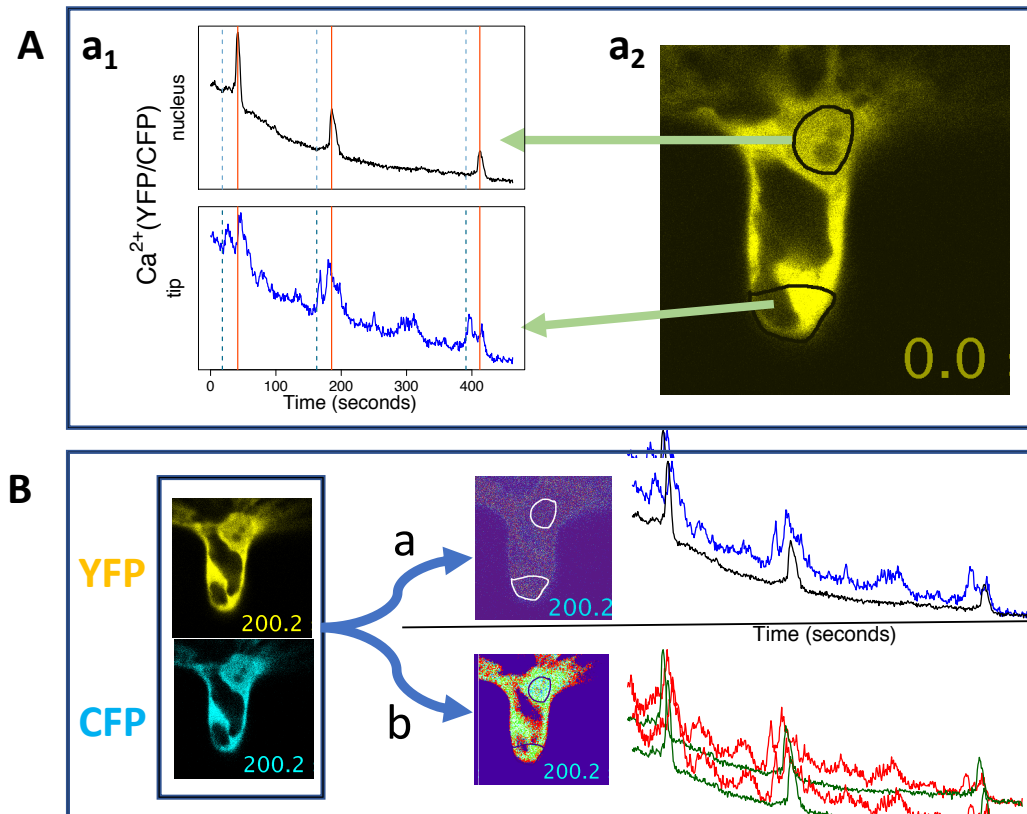


**Figure 6.** Apparent apical and nuclear  $\text{Ca}^{2+}$  spikes are related in a complicated way. Panel (A),  $a_1$ , shows oscillations in perinuclear and apical YFP/CFP ratios, corresponding to the statically-defined regions of interest observed in the image of the root hair YFP signal ( $a_2$ ), where the black region corresponds to the sensor-free vacuole. Panel (B) shows the impact of imaging processing on ratio images ( $t = 200.2$  s) and on the YFP/CFP time series. Option *a*, Panel (B), corresponds to the use of the RatioPlus [61] plugin without background subtraction and without previous filtering of the YFP and CFP images. Option *b*, Panel (B), corresponds to the application of a two-pixel median filter on the YFP and CFP images, followed by the use of RatioPlus with background subtraction and clipping. The time series of Option *a*, Panel (B), are exactly the same (and corresponding to the same times), as those shown in Panel (A),  $a_1$ , with the ratio YFP/CFP at the nucleus in black, superimposed on the ratio at the tip, in blue. The time series corresponding to Option *b*, Panel (B), show the ratio YFP/CFP at the tip in red and the ratio at the nucleus in dark-green. Data were recorded every 0.79 s, and the  $\text{Ca}^{2+}$  sensor was the cytosolic/nuclear-localised YC3.6. Note that although the times at the first and last pixels in an image frame are not exactly the same (because of line scanning), the relation between nuclear and apical traces is not significantly affected by the scanning starting position: if we shift the tip traces by one time point, we do not see any significant difference.

To investigate further, we focussed on the second spike before  $t = 200$  s; see Figure 7A. Whereas the nuclear region of interest seems to capture a fairly stable large area occupied by the sensor (with the exception of the nucleolus), the region of interest at the tip largely coincides with the vacuolar region. Zooming on the tip and the nuclear region, Panel B, Figure 7, we observe that when the precursor apical peak (Point 2,  $t = 168.0$  s) occurs, the brightest (red) pixels in the ratio image are seen in places where there are almost no YFP and CFP signals. This suggests that the apical and perinuclear YFP/CFP

peaks may be caused by different reasons: while perinuclear high ratios may reflect a true increase in  $\text{Ca}^{2+}$  concentration, apical high ratios may have been artefacts of the division between small random numbers, similarly to what we discussed previously (Section 4.1). In fact, the composite apical  $\text{Ca}^{2+}$  spike coincides with a generic drop of both the YFP and CFP intensity, although YFP grows at the time of the major spike (Panel C, Figure 7). Note also that a gradual  $\text{Ca}^{2+}$  growth before the perinuclear  $\text{Ca}^{2+}$  spike coincides with a decay of both YFP and CFP and also with the start of the major apical  $\text{Ca}^{2+}$  spike (grey polygon, Panel C, Figure 7).

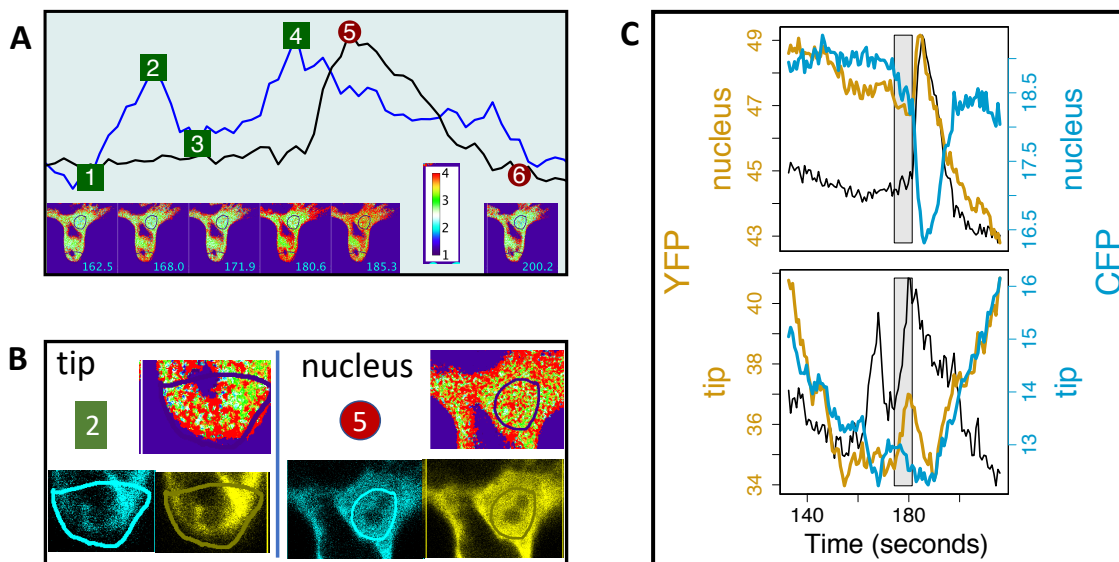


**Figure 7.** Increases in the ratio YFP/CFP may be caused by noise, more so in the apparent *precursor* apical  $\text{Ca}^{2+}$  spike. Panel (A) shows the *second* (before  $t = 200$  s) perinuclear  $\text{Ca}^{2+}$  spike (black), superimposed on the corresponding apparent double apical  $\text{Ca}^{2+}$  spike (blue). Panel (B) shows a snapshot of the YFP, CFP and ratio images at the time of the first apical peak ( $t = 168.0$  s, 2) and of the perinuclear spike ( $t = 185.3$  s, 4): large intensity (red) in the apical ratio image happens at pixels where the apical YFP and CFP images hardly show any signal. Panel (C) shows coincidences (grey polygon) between changes in parallel and antiparallel CFP (cyan) and YFP (gold colour) intensities. Data were recorded every 0.79 s, and the  $\text{Ca}^{2+}$  sensor was the cytosolic/nuclear-localised YC3.6.

It is clear from this example that changes in YFP and CFP intensity can be related in a complex way to  $\text{Ca}^{2+}$  spiking. The existence of perinuclear  $\text{Ca}^{2+}$  spikes is clearly not an artefact, as it coincides with antiparallel YFP and CFP changes, and the same can be said for the second peak of the apical  $\text{Ca}^{2+}$  spike; see Panel C, Figure 7. However, doubts remain about the apparent gradual start of the perinuclear  $\text{Ca}^{2+}$  spike and the *precursor* apical YFP/CFP peak. We can indirectly infer movements and shape changes from parallel (instead of antiparallel) changes in YFP and CFP intensities; see Panel C Figure 7. It could have happened that cytoplasmic streaming led to a decrease of the signal intensity, and a few CFP pixels have fallen below the detection threshold. The partial loss of CFP signal would then artificially increase the YFP/CFP ratio to reveal apparent double apical  $\text{Ca}^{2+}$  spikes. As cytoplasmic streaming also affects the shape and motions of the nucleus, the apparent gradual start of the perinuclear  $\text{Ca}^{2+}$  spike could also be an artefact.

However, even if some YFP/CFP ratio peaks do not indicate true  $\text{Ca}^{2+}$  changes, it is intriguing to observe them so close to each perinuclear  $\text{Ca}^{2+}$  spike. Can cytoplasmic streaming be biologically related to the timing of  $\text{Ca}^{2+}$  release? While previously we saw how results obtained with the use of ratiometric sensors demand a careful interpretation, next we will see how ratiometric sensors can provide additional interesting information, besides the information about  $\text{Ca}^{2+}$  transients.

### 4.3. $Ca^{2+}$ Signals and Other Signals at the Tip

Already several components of the  $Ca^{2+}$  nuclear signalling machinery have been identified, which according to the mathematical models [10] can be enough to sustain periodic oscillations, once  $Ca^{2+}$  spiking is initiated. These mechanistic models are valid if several unknown parameters are tuned adequately. Can imaging reveal any other signal involved in sustaining or initiating  $Ca^{2+}$  spiking?

Figure 8, Panel A, shows perinuclear regular  $Ca^{2+}$  oscillations, imaged using the nuclear/cytosolic sensor YC3.6, in *Medicago truncatula* root hair. At the tip, spiking is hardly visible, and we can barely distinguish a few coincidences between perinuclear  $Ca^{2+}$  spikes and small apical  $Ca^{2+}$  increases. Strikingly, a much more clear relation is found between perinuclear  $Ca^{2+}$  spiking and parallel changes in intensity of YFP and CFP at the tip: they appear synchronised; see Panel B, Figure 8. Naturally, we do not observe oscillations of the YFP and CFP intensities around a certain constant value, as that would have no biological justification. However, we do see a clear coincidence between perinuclear  $Ca^{2+}$  spikes and the speed and/or direction of change in apical YFP and CFP intensities. Since the regions of interest were statically defined at start, these changes are likely to be related to cytoplasmic streaming at the tip; see Panels A and C, Figure 8.

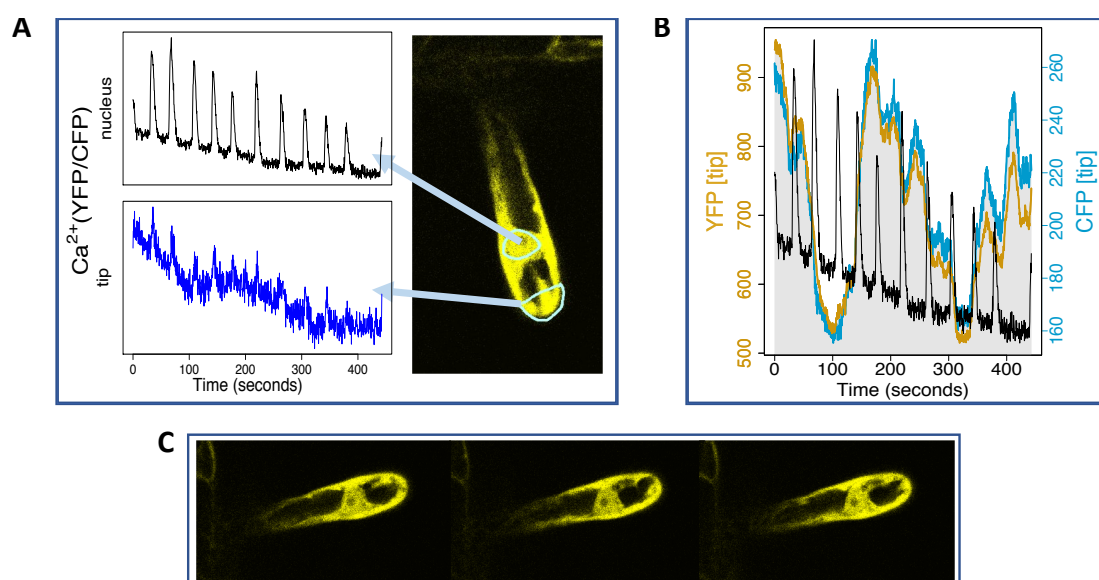


**Figure 8.** Is the  $Ca^{2+}$  signature related to cytoplasmic streaming? Panel (A) shows perinuclear and apical  $Ca^{2+}$  spikes, corresponding to the statically-defined regions shown in the YFP signal. Panel (B) shows that perinuclear  $Ca^{2+}$  spiking occurs when there is a parallel change in the YFP (gold colour) and CFP (cyan) intensities at the tip region. Examples of how the appearance of cytoplasm at the tip changes are seen by comparing Panels (A,C), which show the YFP images at different times. For the time series in Panels (A,B), time points were taken every 0.44 s. The  $Ca^{2+}$  sensor was the cytosolic/nuclear-localised YC3.6.

This example reinforces the idea, advanced in Section 4.2, that there is a relation between motions at the tip region and nuclear  $Ca^{2+}$  spiking. It is presented to stimulate questions. The nucleus and the tip are connected by cytoplasm or cytosolic strands with decreasing degrees of density as the root hair grows older. Although symbiotic  $Ca^{2+}$  spiking is induced by Nod factor and root hair cells can exhibit cytoplasmic streaming without any relation to Nod factor, Sieberer et al. [66] found that patterns of cytoplasmic streaming change with exposure to Nod factor. Can  $Ca^{2+}$  signatures, which are related to the development stage of the root hair [42], be related to specific patterns of cytoplasmic streaming? Is each calcium spike related to mechanical stimuli at the nuclear border? If each spike is related to a rearrangement of the cytoplasm distribution, can this also explain why spikes appear so much noisier at the tip? This could possibly be the case if changes coincided with the temporary appearance of a more web-like cytoplasmic distribution, as this spread would increase the number of

noisier cytoplasm/vacuole interfaces at the tip. Answering these questions would require new images to build robust statistics and also advanced imaging processing methods, which would address the issues raised above.

It is also important to systematically compare results obtained with different imaging techniques (e.g., confocal or wide-field microscopy) and with different sensors (GECIs and dyes, ratiometric and intensimetric).  $\text{Ca}^{2+}$  sensors with improved dynamic range, such as varieties of the GCaMP family [67,68] or GECOs [38], are steadily expanding the choice of  $\text{Ca}^{2+}$  indicators in the plant field. When both the CFP and YFP intensities fall but their ratio increases, intensimetric sensors with a larger dynamic range than YFP could help: if their fluorescence intensity increases in those cases, that indicates a true  $\text{Ca}^{2+}$  change. Therefore, a statistical comparison between results obtained with ratiometric and intensimetric indicators may answer how common it is to observe a *precursor* at the apical region before a nuclear  $\text{Ca}^{2+}$  spike and also whether this precursor is related to motions,  $\text{Ca}^{2+}$  changes or both.

$\text{Ca}^{2+}$  signals in legume-*Rhizobium* symbiosis were recently studied using the intensimetric  $\text{Ca}^{2+}$  indicators R-GECO and G-GECO, which have a much improved dynamic range compared to the yellow cameleons [38]. Since the authors of that study focused on establishing the origin of nuclear  $\text{Ca}^{2+}$  oscillations, they compared intranuclear with perinuclear cytosolic  $\text{Ca}^{2+}$  spikes, rather than systematically comparing perinuclear and apical  $\text{Ca}^{2+}$  spikes. Nevertheless, they showed some intriguing examples of apical and nuclear  $\text{Ca}^{2+}$  spikes. When the cytosol does not fill the entire root hair tip, it is possible to observe at the tip, in a few cases, noisy and small symmetric fluctuations, whose peak corresponds to a nuclear  $\text{Ca}^{2+}$  spike and whose rising phase sometimes begins earlier than the steep rising phase of the nuclear  $\text{Ca}^{2+}$  spike. The noise levels make it impossible to clearly establish if the rising phase corresponds to any type of cytoplasmic streaming effect, movement into focus or increase of the  $\text{Ca}^{2+}$  concentration (the definition of a dynamic region-of-interest, as well as a detailed comparison with the fluctuations of the baseline levels at the nuclear region could perhaps provide more insights). The main point is that all  $\text{Ca}^{2+}$  indicators are affected by signal-to-noise ratio challenges, as soon as we go beyond the simplest applications and focus on cellular regions with very weak signals.

To begin to disentangle biological from spurious correlations, we could start to investigate systematically whether  $\text{Ca}^{2+}$  release and cytoplasmic streaming appear related only at the times when the signal-to-noise ratio decreases. Another point is that *cytoplasmic streaming* should be better characterised. It is not ideal to infer movement from parallel changes in YFP and CFP intensity, as they are affected by a variety of factors, such as photobleaching. Movements and shape changes can, in theory, be characterised easily in binary images. However, in practice, low signal-to-noise ratios can lead to the introduction of additional artefacts when binary masks are created. The decision to create masks or use indirect measurements depends on the balance of which artefacts can be better cancelled, for each particular case.

## 5. Conclusions

We have considered some of the fundamental imaging studies that have informed the current understanding of  $\text{Ca}^{2+}$  signalling during the initiation of legume-bacteria symbiosis. Many of the studies combined imaging with other lines of evidence, from genetic studies to mathematical models. However, each of them contributed to the construction of a coherent narrative of symbiotic calcium signalling based on imaging. They supported the idea of two symbiotic  $\text{Ca}^{2+}$  signals: a  $\text{Ca}^{2+}$  flux at the root hair tip and nuclear  $\text{Ca}^{2+}$  oscillations with different frequencies characteristic of different symbiotic phenomena.

Historically, fluorescence microscopy was a qualitative technique, valuable for stimulation of new avenues of research or for visual illustration of evidence backed by other methods. In recent years, and in parallel with advances in high-resolution microscopy and the development of new fluorescent sensors, bioimaging has been fast progressing from direct observation to quantification,

with new methods serving to estimate and reduce the uncertainty in the imaging data [16]. Here, we have reviewed the literature and attempted to identify challenges and potential pitfalls. Regarding the legume-rhizobial symbiosis, one source of uncertainty arises from the comparison between  $\text{Ca}^{2+}$  signals in cellular regions disproportionately affected by noise: the problematic regions are nuclear periphery affected by a low signal-to-noise ratio at edge artefacts, and the root hair tip that is affected by cytoplasmic streaming.

Shedding light onto the consequences of image processing approaches, we suggest that  $\text{Ca}^{2+}$  spiking is not as localised as commonly thought. Regarding intranuclear  $\text{Ca}^{2+}$ , its stronger concentration at the nuclear periphery is not presently confirmed by robust image processing approaches. That does not invalidate the fact that the  $\text{Ca}^{2+}$  signalling machinery is localised at the nuclear membranes; instead, it questions its limited reach. The apparent dissipation of  $\text{Ca}^{2+}$  spiking with the distance from the nucleus could possibly be explained by an increased signal-to-noise ratio at the tip caused by cytoplasmic streaming. A detailed comparison between *degraded* apical  $\text{Ca}^{2+}$  spikes with *sharp* perinuclear  $\text{Ca}^{2+}$  spikes reveals unexpected correlations: in some cases, an apparent apical  $\text{Ca}^{2+}$  spike seems to precede a perinuclear  $\text{Ca}^{2+}$  spike. However, we note that when measuring small apparent  $\text{Ca}^{2+}$  transients by ratiometric sensors, sometimes we are unable to rule out artefacts: e.g., cytoplasmic streaming can cause the CFP signal to become partially undetectable, leading to artificially high YFP/CFP ratios. Does cytoplasmic streaming merely affect the measurement of  $\text{Ca}^{2+}$  signals or does it affect the  $\text{Ca}^{2+}$  signals themselves, as it sometimes appears to interfere at particular moments, at the start of a spike? We show one example where the most unequivocal relation is not between apical and perinuclear  $\text{Ca}^{2+}$  signals, but between changes in apical cytoplasmic streaming and the frequency of perinuclear  $\text{Ca}^{2+}$  signals. If confirmed by future studies, this will show that the entire root hair participates in  $\text{Ca}^{2+}$  spiking throughout its duration.

For the interdisciplinary synergy that is key in bioimaging, biological expertise should be complemented by the skills of physicists, computational scientists and microscopy specialists. Computational methods would help formalise and standardise reproducible imaging protocols, with estimation of uncertainties [69]. Microscopy specialists would help understand the noisy features hidden in the images. The contribution of physicists working in the area of complex systems could help elucidate ideas like cell autonomy: nuclear  $\text{Ca}^{2+}$  spiking is thought to be cell-autonomous, but, per se, frequency mismatch does not imply independence [70], as nonlinear interactions can manifest in unexpected ways. A complex systems approach could also help in determining the precise way (mechanical effects, transport of biochemical stimulus, particular patterns) [71] in which cytoplasmic streaming is (or not) related to the  $\text{Ca}^{2+}$  spiking rhythm.

**Author Contributions:** Conceptualization, T.V.M.; methodology, T.V.M. and V.N.L.; investigation, T.V.M.; writing and review and editing, T.V.M. and V.N.L.

**Funding:** This research was funded by BBSRC's Institute Strategic Programme on Biotic Interactions underpinning Crop Productivity (BB/J004553/1) and Plant Health (BB/P012574/1).

**Acknowledgments:** T.V.M. acknowledges Sarah Shailes, Sylvia Singh, Grant Calder, and Jongho Sun for advice on plant preparation and confocal microscopy. We acknowledge Richard J. Morris and Allan Downie for very helpful comments.

**Conflicts of Interest:** The authors declare no conflict of interest. The funding sponsors had no role in the design of the study; in the collection, analyses, or interpretation of data; in the writing of the manuscript; nor in the decision to publish the results.

## Abbreviations

The following abbreviations are used in this manuscript:

OG	Oregon Green
TR	Texas Red
Nod	Nodulation
FP	Fluorescent Protein

FRET	Förster (or Fluorescence) Resonance Energy Transfer
YC	Yellow Cameleon
YFP	Yellow Fluorescent Protein
CFP	Cyan Fluorescent Protein
GECI	Genetically-Encoded Calcium Indicator
CLSM	Confocal Laser Scanning Microscopy

## References

- Downie, J.A. Legume nodulation. *Curr. Biol.* **2014**, *24*, R184–R190. [[PubMed](#)]
- Oldroyd, G.E.; Murray, J.D.; Poole, P.S.; Downie, J.A. The Rules of Engagement in the Legume-Rhizobial Symbiosis. *Annu. Rev. Genet.* **2011**, *45*, 119–144. [[CrossRef](#)]
- Fournier, J.; Timmers, A.C.J.; Sieberer, B.J.; Jauneau, A.; Chabaud, M.; Barker, D.G. Mechanism of infection thread elongation in root hairs of *Medicago truncatula* and dynamic interplay with associated rhizobial colonization. *Plant Physiol.* **2008**, *148*, 1985–1995. [[CrossRef](#)] [[PubMed](#)]
- Newman-Griffis, A.H.; del Cerro, P.; Charpentier, M.; Meier, I. *Medicago* LINC complexes function in nuclear morphology, nuclear movement, and root nodule symbiosis. *Plant Physiol.* **2019**, *179*, 491–506. [[CrossRef](#)] [[PubMed](#)]
- Palmer, A.E.; Tsien, R.Y. Measuring calcium signaling using genetically targetable fluorescent indicators. *Nat. Protoc.* **2006**, *1*, 1057. [[CrossRef](#)] [[PubMed](#)]
- Kanchiswamy, C.N.; Malnoy, M.; Occhipinti, A.; Maffei, M.E. Calcium imaging perspectives in plants. *Int. J. Mol. Sci.* **2014**, *15*, 3842–3859. [[CrossRef](#)]
- Walia, A.; Waadt, R.; Jones, A.M. Genetically Encoded Biosensors in Plants: Pathways to Discovery. *Annu. Rev. Plant Biol.* **2018**, *69*, 497–524. [[CrossRef](#)]
- Behera, S.; Krebs, M.; Loro, G.; Schumacher, K.; Costa, A.; Kudla, J.  $Ca^{2+}$  Imaging in Plants Using Genetically Encoded Yellow Cameleon  $Ca^{2+}$  Indicators. *Cold Spring Harb. Protoc.* **2013**, *2013*, pdb.top066183. [[CrossRef](#)]
- Hilleary, R.; Choi, W.G.; Kim, S.H.; Lim, S.D.; Gilroy, S. Sense and sensibility: The use of fluorescent protein-based genetically encoded biosensors in plants. *Curr. Opin. Plant Biol.* **2018**, *46*, 32–38. [[CrossRef](#)]
- Charpentier, M.; Martins, T.V.; Granqvist, E.; Oldroyd, G.E.; Morris, R.J. The role of DMI1 in establishing  $Ca^{2+}$  oscillations in legume symbioses. *Plant Signal. Behav.* **2013**, *8*, e22894. [[CrossRef](#)]
- Martins, T.V.; Evans, M.J.; Wysham, D.B.; Morris, R.J. Nuclear pores enable sustained perinuclear calcium oscillations. *BMC Syst. Biol.* **2016**, *10*, 55. [[CrossRef](#)]
- Oldroyd, G.E.D. Speak, friend, and enter: Signalling systems that promote beneficial symbiotic associations in plants. *Nat. Rev. Microbiol.* **2013**, *11*, 252–263. [[CrossRef](#)]
- Charpentier, M. Calcium signals in the plant nucleus: Origin and function. *J. Exp. Bot.* **2018**, *69*, 4165–4173. [[CrossRef](#)]
- Aldon, D.; Mbengue, M.; Mazars, C.; Galaud, J.P. Calcium Signalling in Plant Biotic Interactions. *Int. J. Mol. Sci.* **2018**, *19*, 665. [[CrossRef](#)]
- Kudla, J.; Becker, D.; Grill, E.; Hedrich, R.; Hippler, M.; Kummer, U.; Parniske, M.; Romeis, T.; Schumacher, K. Advances and current challenges in calcium signaling. *New Phytol.* **2018**, *218*, 414–431. [[CrossRef](#)]
- Sbalzarini, I.F. Seeing Is Believing: Quantifying Is Convincing: Computational Image Analysis in Biology. In *Focus on Bio-Image Informatics*; De Vos, W.H., Munck, S., Timmermans, J.P., Eds.; Springer International Publishing: Cham, Switzerland, 2016; pp. 1–39.
- Nketia, T.A.; Sailem, H.; Rohde, G.; Machiraju, R.; Rittscher, J. Analysis of live cell images: Methods, tools and opportunities. *Methods* **2017**, *115*, 65–79. [[CrossRef](#)]
- McAinsh, M.R.; Pittman, J.K. Shaping the calcium signature. *New Phytol.* **2009**, *181*, 275–294. [[CrossRef](#)]
- Yuan, P.; Jauregui, E.; Du, L.; Tanaka, K.; Poovaiah, B. Calcium signatures and signaling events orchestrate plant–microbe interactions. *Curr. Opin. Plant Biol.* **2017**, *38*, 173–183. [[CrossRef](#)]
- Whalley, H.J.; Knight, M.R. Calcium signatures are decoded by plants to give specific gene responses. *New Phytol.* **2013**, *197*, 690–693. [[CrossRef](#)]
- Kudla, J.; Batic, O.; Hashimoto, K. Calcium signals: The lead currency of plant information processing. *Plant Cell* **2010**, *22*, 541–563. [[CrossRef](#)]

22. Koldenkova, V.P.; Nagai, T. Genetically encoded  $\text{Ca}^{2+}$  indicators: Properties and evaluation. *Biochim. Biophys. Acta (BBA) Mol. Cell Res.* **2013**, *1833*, 1787–1797. [[CrossRef](#)] [[PubMed](#)]
23. Himschoot, E.; Krebs, M.; Costa, A.; Beeckman, T.; Vanneste, S. Calcium Ion Dynamics in Roots: Imaging and Analysis. In *Root Development: Methods and Protocols*; Ristova, D., Barbez, E., Eds.; Springer: New York, NY, USA, 2018; pp. 115–130.
24. Miyawaki, A.; Llopis, J.; Heim, R.; McCaffery, J.M.; Adams, J.A.; Ikura, M.; Tsien, R.Y. Fluorescent indicators for  $\text{Ca}^{2+}$  based on green fluorescent proteins and calmodulin. *Nature* **1997**, *388*, 882. [[CrossRef](#)]
25. Krebs, M.; Held, K.; Binder, A.; Hashimoto, K.; Den Herder, G.; Parniske, M.; Kudla, J.; Schumacher, K. FRET-based genetically encoded sensors allow high-resolution live cell imaging of  $\text{Ca}^{2+}$  dynamics. *Plant J.* **2012**, *69*, 181–192. [[CrossRef](#)] [[PubMed](#)]
26. Bankhead, P. Analyzing Fluorescence Microscopy Images with ImageJ. 2014. Available online: [https://sydney.edu.au/medicine/bosch/facilities/advanced-microscopy/user-support/ImageJ\\_FL\\_Image\\_Analysis.pdf](https://sydney.edu.au/medicine/bosch/facilities/advanced-microscopy/user-support/ImageJ_FL_Image_Analysis.pdf) (accessed on 21 January 2019).
27. Sheppard, Colin J.R. Gan, X.; Gu, M.; Roy, M. Signal-to-noise ratio in confocal microscopes. In *Handbook of Biological Confocal Microscopy*; Pawley, J.B., Ed.; Springer Science + Business Media LLC: New York, NY, USA, 2006; pp. 442–451.
28. Cárdenas, L.; Feijó, J.A.; Kunkel, J.G.; Sánchez, F.; Holdaway-Clarke, T.; Hepler, P.K.; Quinto, C. Rhizobium Nod factors induce increases in intracellular free calcium and extracellular calcium influxes in bean root hairs. *Plant J.* **1999**, *19*, 347–352. [[CrossRef](#)] [[PubMed](#)]
29. Norbert, C.D.; Rook, M.B.; Bisseling, T.; Emons, A.M.C. Lipochito-oligosaccharides re-initiate root hair tip growth in *Vicia sativa* with high calcium and spectrin-like antigen at the tip. *Plant J.* **1998**, *13*, 341–350.
30. Gehring, C.A.; Irving, H.R.; Kabbara, A.A.; Parish, R.W.; Boukli, N.M.; Broughton, W.J. Rapid, Plateau-like Increases in Intracellular Free Calcium Are Associated with Nod-Factor-Induced Root-Hair Deformation. *Mol. Plant-Microbe Interact.* **1997**, *10*, 791–802. [[CrossRef](#)]
31. Shaw, S.L.; Long, S.R. Nod Factor Elicits Two Separable Calcium Responses in *Medicago truncatula* Root Hair Cells. *Plant Physiol.* **2003**, *131*, 976–984. [[CrossRef](#)] [[PubMed](#)]
32. Morieri, G.; Martinez, E.A.; Jarynowski, A.; Driguez, H.; Morris, R.; Oldroyd, G.E.D.; Downie, J.A. Host-specific Nod-factors associated with *Medicago truncatula* nodule infection differentially induce calcium influx and calcium spiking in root hairs. *New Phytol.* **2013**, *200*, 656–662. [[CrossRef](#)]
33. Miwa, H.; Sun, J.; Oldroyd, G.E.D.; Downie, J.A. Analysis of Nod-Factor-Induced Calcium Signaling in Root Hairs of Symbiotically Defective Mutants of *Lotus japonicus*. *Mol. Plant-Microbe Interact.* **2006**, *19*, 914–923. [[CrossRef](#)]
34. Sieberer, B.J.; Chabaud, M.; Timmers, A.C.; Monin, A.; Fournier, J.; Barker, D.G. A nuclear-targeted cameleon demonstrates intranuclear  $\text{Ca}^{2+}$  spiking in *Medicago truncatula* root hairs in response to rhizobial nodulation factors. *Plant Physiol.* **2009**, *151*, 1197–1206. [[CrossRef](#)]
35. Capoen, W.; Sun, J.; Wysham, D.; Otegui, M.S.; Venkateshwaran, M.; Hirsch, S.; Miwa, H.; Downie, J.A.; Morris, R.J.; Ané, J.M.; et al. Nuclear membranes control symbiotic calcium signaling of legumes. *Proc. Natl. Acad. Sci. USA* **2011**, *108*, 14348–14353. [[CrossRef](#)]
36. Ehrhardt, D.W.; Wais, R.; Long, S.R. Calcium spiking in plant root hairs responding to *Rhizobium* nodulation signals. *Cell* **1996**, *85*, 673–681. [[CrossRef](#)]
37. Walker, S.A.; Viprey, V.; Downie, J.A. Dissection of nodulation signaling using pea mutants defective for calcium spiking induced by Nod factors and chitin oligomers. *Proc. Natl. Acad. Sci. USA* **2000**, *97*, 13413–13418. [[CrossRef](#)]
38. Kelner, A.; Leitão, N.; Chabaud, M.; Charpentier, M.; de Carvalho-Niebel, F. Dual Color Sensors for Simultaneous Analysis of Calcium Signal Dynamics in the Nuclear and Cytoplasmic Compartments of Plant Cells. *Front. Plant Sci.* **2018**, *9*, 245. [[CrossRef](#)]
39. Oldroyd, G.E.; Downie, J.A. Nuclear calcium changes at the core of symbiosis signalling. *Curr. Opin. Plant Biol.* **2006**, *9*, 351–357. [[CrossRef](#)] [[PubMed](#)]
40. Edel, K.H.; Marchadier, E.; Brownlee, C.; Kudla, J.; Hetherington, A.M. The Evolution of Calcium-Based Signalling in Plants. *Curr. Biol.* **2017**, *27*, R667–R679. [[CrossRef](#)]
41. Wais, R.J.; Galera, C.; Oldroyd, G.; Catoira, R.; Penmetza, R.V.; Cook, D.; Gough, C.; Dénarié, J.; Long, S.R. Genetic analysis of calcium spiking responses in nodulation mutants of *Medicago truncatula*. *Proc. Natl. Acad. Sci. USA* **2000**, *97*, 13407–13412. [[CrossRef](#)] [[PubMed](#)]

42. Miwa, H.; Sun, J.; Oldroyd, G.E.D.; Downie, J.A. Analysis of calcium spiking using aameleon calcium sensor reveals that nodulation gene expression is regulated by calcium spike number and the developmental status of the cell. *Plant J.* **2006**, *48*, 883–894. [[CrossRef](#)]
43. Sun, J.; Miwa, H.; Downie, J.A.; Oldroyd, G.E. Mastoparan Activates Calcium Spiking Analogous to Nod Factor-Induced Responses in *Medicago truncatula* Root Hair Cells. *Plant Physiol.* **2007**, *144*, 695–702. [[CrossRef](#)]
44. Harris, J.M.; Wais, R.; Long, S.R. Rhizobium-Induced Calcium Spiking in *Lotus japonicus*. *Mol. Plant-Microbe Interact.* **2003**, *16*, 335–341. [[CrossRef](#)] [[PubMed](#)]
45. Capoen, W.; Den Herder, J.; Sun, J.; Verplancke, C.; De Keyser, A.; De Rycke, R.; Goormachtig, S.; Oldroyd, G.; Holsters, M. Calcium Spiking Patterns and the Role of the Calcium/Calmodulin-Dependent Kinase CcAMK in Lateral Root Base Nodulation of *Sesbania rostrata*. *Plant Cell* **2009**, *21*, 1526–1540. [[CrossRef](#)]
46. Sieberer, B.J.; Chabaud, M.; Fournier, J.; Timmers, A.C.; Barker, D.G. A switch in Ca<sup>2+</sup> spiking signature is concomitant with endosymbiotic microbe entry into cortical root cells of *Medicago truncatula*. *Plant J.* **2012**, *69*, 822–830. [[CrossRef](#)]
47. Charpentier, M.; Bredemeier, R.; Wanner, G.; Takeda, N.; Schleiff, E.; Parniske, M. *Lotus japonicus* CASTOR and POLLUX are ion channels essential for perinuclear calcium spiking in legume root endosymbiosis. *Plant Cell* **2008**, *20*, 3467–3479. [[CrossRef](#)]
48. Charpentier, M.; Sun, J.; Martins, T.V.; Radhakrishnan, G.V.; Findlay, K.; Soumpourou, E.; Thouin, J.; Véry, A.A.; Sanders, D.; Morris, R.J.; et al. Nuclear-localized cyclic nucleotide-gated channels mediate symbiotic calcium oscillations. *Science* **2016**, *352*, 1102–1105. [[CrossRef](#)]
49. Saito, K.; Yoshikawa, M.; Yano, K.; Miwa, H.; Uchida, H.; Asamizu, E.; Sato, S.; Tabata, S.; Imaizumi-Anraku, H.; Umehara, Y.; et al. NUCLEOPORIN85 is required for calcium spiking, fungal and bacterial symbioses, and seed production in *Lotus japonicus*. *Plant Cell* **2007**, *19*, 610–624. [[CrossRef](#)]
50. Shailes, S. Regulation of Calcium Influx and Reactive Oxygen Species Production during Infection of Legumes by Rhizobia. Ph.D. Thesis, University of East Anglia, Norwich, UK, 2014.
51. Gage, D.J. Infection and invasion of roots by symbiotic, nitrogen-fixing rhizobia during nodulation of temperate legumes. *Microbiol. Mol. Biol. Rev.* **2004**, *68*, 280–300. [[CrossRef](#)]
52. Monshausen, G.B.; Messerli, M.A.; Gilroy, S. Imaging of the Yellow Cameleon 3.6 Indicator Reveals That Elevations in Cytosolic Ca<sup>2+</sup> Follow Oscillating Increases in Growth in Root Hairs of *Arabidopsis*. *Plant Physiol.* **2008**, *147*, 1690–1698. [[CrossRef](#)]
53. Mendrinna, A.; Persson, S. Root hair growth: It's a one way street. *F1000Prime Rep.* **2015**, *7*, 23–23. [[CrossRef](#)]
54. Sieberer, B.J.; Fournier, J.; Timmers, A.C.; Chabaud, M.; Barker, D.G. Nuclear Ca<sup>2+</sup> Signaling Reveals Active Bacterial-Host Communication Throughout Rhizobial Infection in Root Hairs of *Medicago truncatula*. In *Biological Nitrogen Fixation*; de Bruijn, F.J., Ed.; John Wiley and Sons, Ltd.: 2015; Chapter 57, pp. 567–574.
55. Kosuta, S.; Hazledine, S.; Sun, J.; Miwa, H.; Morris, R.J.; Downie, J.A.; Oldroyd, G.E.D. Differential and chaotic calcium signatures in the symbiosis signaling pathway of legumes. *Proc. Natl. Acad. Sci. USA* **2008**, *105*, 9823–9828. [[CrossRef](#)]
56. Granqvist, E.; Wysham, D.; Hazledine, S.; Kozlowski, W.; Sun, J.; Charpentier, M.; Martins, T.V.; Haleux, P.; Tsaneva-Atanasova, K.; Downie, J.A.; et al. Buffering Capacity Explains Signal Variation in Symbiotic Calcium Oscillations. *Plant Physiol.* **2012**, *160*, 2300–2310. [[CrossRef](#)]
57. Marhl, M.; Perc, M.; Schuster, S. A minimal model for decoding of time-limited Ca<sup>2+</sup> oscillations. *Biophys. Chem.* **2006**, *120*, 161–167. [[CrossRef](#)] [[PubMed](#)]
58. Pawley, J.B. *Handbook of Biological Confocal Microscopy*; Springer Science + Business Media LLC: New York, NY, USA, 2006.
59. Volcano Dataset. Available online: <https://stat.ethz.ch/R-manual/R-devel/library/datasets/html/volcano.html> (accessed on 21 January 2019).
60. Soetaert, K. plot3D Package. Available online: <https://cran.r-project.org/web/packages/plot3D/index.html> (accessed on 21 January 2019).
61. Magalhaes, P. RatioPlus Plugin. Available online: <https://imagej.nih.gov/ij/plugins/ratio-plus.html> (accessed on 14 January 2019).
62. Schneider, C.A.; Rasband, W.S.; Eliceiri, K.W. NIH Image to ImageJ: 25 years of image analysis. *Nat. Methods* **2012**, *9*, 671. [[CrossRef](#)]

63. Rudolf, R.; Mongillo, M.; Magalhães, P.J.; Pozzan, T. In vivo monitoring of Ca<sup>2+</sup> uptake into mitochondria of mouse skeletal muscle during contraction. *J. Cell Biol.* **2004**, *166*, 527–536. [CrossRef]
64. Rudolf, R.; Magalhães, P.J.; Pozzan, T. Direct in vivo monitoring of sarcoplasmic reticulum Ca<sup>2+</sup> and cytosolic cAMP dynamics in mouse skeletal muscle. *J. Cell Biol.* **2006**, *173*, 187–193. [CrossRef] [PubMed]
65. Bootman, M.D.; Rietdorf, K.; Collins, T.; Walker, S.; Sanderson, M. Ca<sup>2+</sup>-Sensitive Fluorescent Dyes and Intracellular Ca<sup>2+</sup> Imaging. *Cold Spring Harb. Protoc.* **2013**, *2013*, pdb.top066050. [CrossRef]
66. Sieberer, B.; Emons, A.M.C. Cytoarchitecture and pattern of cytoplasmic streaming in root hairs of *Medicago truncatula* during development and deformation by nodulation factors. *Protoplasma* **2000**, *214*, 118–127. [CrossRef]
67. Nakai, J.; Ohkura, M.; Imoto, K. A high signal-to-noise Ca<sup>2+</sup> probe composed of a single green fluorescent protein. *Nat. Biotechnol.* **2001**, *19*, 137. [CrossRef]
68. Toyota, M.; Spencer, D.; Sawai-Toyota, S.; Jiaqi, W.; Zhang, T.; Koo, A.J.; Howe, G.A.; Gilroy, S. Glutamate triggers long-distance, calcium-based plant defense signaling. *Science* **2018**, *361*, 1112–1115. [CrossRef]
69. Evaluation of Measurement Data—Guide to the Expression of Uncertainty in Measurement JCGM 100:2008. (GUM 1995 with Minor Corrections), 2008. Available online: [http://www.bipm.org/utis/common/documents/jcgm/JCGM\\_100\\_2008\\_E.pdf](http://www.bipm.org/utis/common/documents/jcgm/JCGM_100_2008_E.pdf) (accessed on 17 February 2019).
70. Pikovsky, A.; Rosenblum, M.; Kurths, J. *Synchronization: A Universal Concept in Nonlinear Sciences*; Cambridge Nonlinear Science Series, Cambridge University Press: Cambridge, UK, 2001.
71. Goldstein, R.E.; van de Meent, J.W. A physical perspective on cytoplasmic streaming. *Interface Focus* **2015**, *5*, 20150030. [CrossRef] [PubMed]



© 2019 by the authors. Licensee MDPI, Basel, Switzerland. This article is an open access article distributed under the terms and conditions of the Creative Commons Attribution (CC BY) license (<http://creativecommons.org/licenses/by/4.0/>).